

Antiferromagnetic Tunnel Junctions for Spintronics

Ding-Fu Shao^{1,*} and Evgeny Y. Tsymbal^{2,†}

¹ Key Laboratory of Materials Physics, Institute of Solid State Physics, HFIPS, Chinese Academy of Sciences, Hefei 230031, China

² Department of Physics and Astronomy & Nebraska Center for Materials and Nanoscience, University of Nebraska, Lincoln, Nebraska 68588-0299, USA

*dfshao@issp.ac.cn; † tsymbal@unl.edu

Abstract Antiferromagnetic (AFM) spintronics has emerged as a subfield of spintronics, where an AFM Néel vector is used as a state variable. Efficient electric control and detection of the Néel vector are critical for spintronic applications. This review article features fundamental properties of AFM tunnel junctions (AFMTJs) as spintronic devices where such electric control and detection can be realized. We emphasize critical requirements for observing a large tunneling magnetoresistance (TMR) effect in AFMTJs with collinear and noncollinear AFM electrodes, such as a momentum-dependent spin polarization and Néel spin currents. We further discuss spin torques in AFMTJs that are capable of Néel vector switching. Overall, AFMTJs have potential to become a new standard for spintronics providing larger magnetoresistive effects, few orders of magnitude faster switching speed, and much higher packing density than conventional magnetic tunnel junctions (MTJs).

1. Introduction

Spintronics is a vigorously developing field of electronics, where electron's spin controls device functionality [1]. Conventional schemes rely on magnetic tunnel junctions (MTJs)—key devices of modern spintronic technologies, such as magnetic random-access memories (MRAMs) (Fig. 1a). In an MRAM, MTJs carry information bits, that can be written-in and read-out by electric means. An important advantage of an MRAM is its non-volatility; however, it is deficient with its low switching speed that is determined by the time required to rotate the magnetization of a ferromagnet, which is typically a few nanoseconds (Fig. 1a). This is nearly three orders of magnitude slower than charging a capacitor in CMOS technologies.

Antiferromagnetic (AFM) spintronics has recently emerged as a subfield of spintronics, where an AFM order parameter known as the Néel vector is used as a state variable [2-4]. Due to being robust against magnetic perturbations, producing no stray fields, and exhibiting ultrafast dynamics, antiferromagnets can serve as promising functional materials for spintronic applications [5]. Potentially, antiferromagnets can replace ferromagnets due to their orders of magnitude enhanced switching speed and storage density. To realize this potential, efficient electric control and detection of the AFM Néel vector are required. These functionalities can be realized using AFM tunnel junctions (AFMTJs) as core spintronic devices. The recent theoretical predictions [6 - 8] and experimental demonstrations [9,10] show that AFMTJs can exhibit a strong electric response to the state of the Néel vector, and that the Néel vector itself can be electrically controlled [11]. Potentially, AFM random-access memories (AFM-RAMs) are envisioned (Fig. 1b) that can provide a stronger magnetoresistive response, much faster operation speed, and higher memory density than MRAMs. This review article features fundamental properties of collinear and noncollinear AFMTJs, such as a momentum-dependent spin

polarization and Néel spin currents, that control their magnetoresistive properties and discusses spin torques in AFMTJs that are capable of Néel vector switching.

2. Magnetic tunnel junctions and tunneling magnetoresistance

A ferromagnet hosts exchange-coupled parallel-aligned magnetic moments carrying a finite magnetization (Fig. 2a), which can be used as a state variable to encode the information. Magnetization is easily controlled by magnetic fields and spin torques, which allows convenient write-in of information. The non-vanishing magnetization in a ferromagnet is inherited from its exchange-split electronic band structure (Figs. 2b and 2c) that is also responsible for a variety of useful spin-dependent transport properties [1]. Among them are those (e.g., magnetoresistance) that allow the electrical detection of the magnetization state for information read-out. To date, most spintronic devices have been based on ferromagnets.

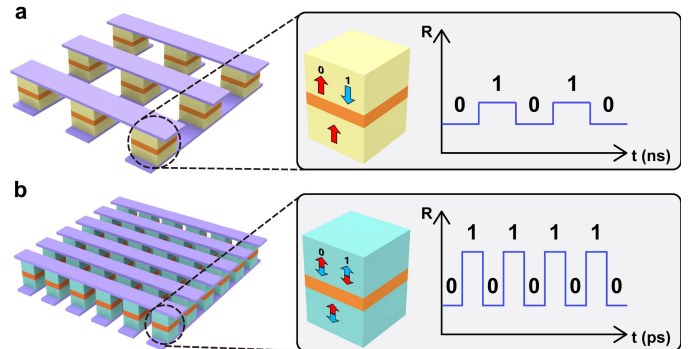


FIG. 1 (a) Schematic of MRAM consisting of an array of conventional MTJs. (b) Schematic of AFM-RAM consisting of an array of AFMTJs. AFM-RAMs are expected to exhibit a stronger magnetoresistive response, a much faster operation speed, and higher density compared to the conventional MRAM, due to the advantages of AFMTJs.

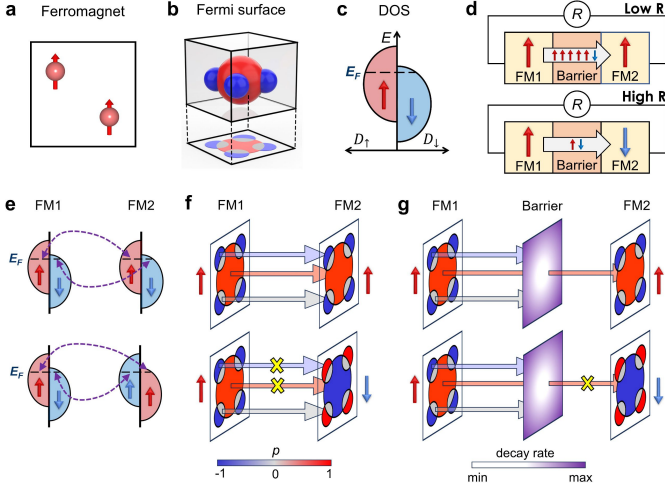


FIG. 2 (a-c) Schematic of magnetic structure (a), Fermi surface (b), and electronic density of states (DOS) (c) of a ferromagnet. Red and blue colors in (b) denote up- and down-spin Fermi surfaces. Projection of the Fermi surface into a 2D Brillouin zone represents a distribution of conduction channels. (d) Schematic of a conventional MTJ based on two FM electrodes and a nonmagnetic tunnel barrier. (e) Schematic of the TMR mechanism based on spin-polarized DOS. (f) Schematic of the TMR mechanism based on the momentum-dependent spin-polarization matching of conduction channels in two electrodes. (g) Schematic of momentum-dependent spin-filtering in the tunnel barrier.

Magnetic tunnel junctions (MTJs) An MTJ is the most common spintronic device utilizing the advantages of ferromagnets. Figure 2d shows schematics of an MTJ, where left and right electrodes are ferromagnetic (FM) metals separated by an insulating non-magnetic tunnel barrier. Magnetization of the left electrode is pinned, while it is free in the right electrode. Parallel (P) and antiparallel (AP) alignments of magnetization in the two electrodes represent “0” and “1” bits of information.

Tunneling magnetoresistance (TMR) Electron tunneling in an MTJ can be effectively controlled by the relative orientation of magnetization. Switching between the P and AP states changes the resistance of an MTJ. This effect is known as tunneling magnetoresistance (TMR) and can be used for read-out of “0s” and “1s” in an MTJ [12,13]. The magnitude of the effect is normally quantified by the TMR ratio, $TMR = \frac{R_{AP} - R_P}{R_P}$, where R_P (R_{AP}) is resistance of the P (AP) state. TMR can be understood assuming that electron’s spin is conserved in the tunneling process, so that tunneling of up- and down-spin electrons occurs in parallel in two spin conduction channels [14]. As a result, TMR can be qualitatively described in terms of Julliere’s formula $TMR = \frac{2p_1p_2}{1-p_1p_2}$, where p_1 and p_2 are spin polarizations of the two electrodes [12]. The widely used definition of the total spin polarization is $p = \frac{D^\uparrow(E_F) - D^\downarrow(E_F)}{D^\uparrow(E_F) + D^\downarrow(E_F)}$,

where $D^{\uparrow,\downarrow}(E_F)$ is the spin-dependent density of states (DOS) at the Fermi energy (E_F) (Figs. 2c and 2e). Based on this formula, a larger spin polarization of the electrodes favors a larger TMR. While relevant for polycrystalline MTJs, this simple description does not capture anisotropy of the Fermi surface that is essential for tunneling in crystalline MTJs, and it does not reflect effects of the tunnel barrier and interfaces [15].

In crystalline MTJs with no diffuse scattering, tunneling conductance G can be described in the ballistic transport regime where the transverse wave vector \mathbf{k}_\perp is conserved, so that [16,17]

$$G = \sum_{\sigma} G^{\sigma} = \frac{e^2}{(2\pi)^3 \hbar} \sum_{\sigma} \int T_{\parallel}^{\sigma} d\mathbf{k}_{\parallel}, \quad (1)$$

where σ is the spin index, and T_{\parallel}^{σ} is the \mathbf{k}_{\parallel} - and σ -dependent transmission. T_{\parallel}^{σ} is determined by the probability of tunneling of the Bloch states across the barrier at \mathbf{k}_{\parallel} . Due to being separated into \mathbf{k}_{\parallel} -dependent channels conducting in parallel, the spin-dependent conductance in MTJs can be better characterized in terms of the \mathbf{k}_{\parallel} -dependent number of conduction channels $N_{\parallel}^{\sigma}(\mathbf{k}_{\parallel})$ in the electrodes, rather than the total DOS—a characteristic integrated over \mathbf{k}_{\parallel} . The number of conduction channels is defined by the number of propagating Bloch states in the transport direction at the Fermi energy [18]:

$$N_{\parallel}^{\sigma}(\mathbf{k}_{\parallel}) = \frac{\hbar}{2} \sum_n \int |v_{nz}^{\sigma}| \frac{\partial f}{\partial E_n^{\sigma}(\mathbf{k})} dk_z, \quad (2)$$

where $E_n^{\sigma}(\mathbf{k})$ is energy of the n -th band, $v_{nz}^{\sigma} = \frac{\partial E_n^{\sigma}(\mathbf{k})}{\hbar \partial k_z}$ is the band velocity along the transport z direction, and f is the Fermi distribution function. A \mathbf{k}_{\parallel} -dependent spin polarization p_{\parallel} can then be defined by

$$p_{\parallel}(\mathbf{k}_{\parallel}) = \frac{N_{\parallel}^{\uparrow} - N_{\parallel}^{\downarrow}}{N_{\parallel}^{\uparrow} + N_{\parallel}^{\downarrow}}, \quad (3)$$

and the net spin polarization by

$$p = \frac{\sum_{\mathbf{k}_{\parallel}} (N_{\parallel}^{\uparrow} - N_{\parallel}^{\downarrow})}{\sum_{\mathbf{k}_{\parallel}} (N_{\parallel}^{\uparrow} + N_{\parallel}^{\downarrow})}. \quad (4)$$

These quantities capture electron’s spin and velocity at the Fermi surface, and thus are more relevant for the description of transport properties than the DOS. They can be regarded as *transport spin polarizations* of a magnetic metal in the ballistic transport regime. In crystalline MTJs, the \mathbf{k}_{\parallel} -dependent transport spin polarization p_{\parallel} is more appropriate to quantify TMR than the net spin polarization p . Based on p_{\parallel} , TMR in crystalline MTJs can be explained by stronger transmission for a P magnetization state than for an AP state due to the matching of $p_{\parallel,1}$ and $p_{\parallel,2}$ in the two electrodes (labeled by 1 and 2) for the P state and mismatching for the AP state (Fig. 2e).

The tunneling barrier also plays an important role in TMR. First, transmission is expected to be stronger at those \mathbf{k}_{\parallel} where the decay rate in the barrier is lower. Second, barrier effectively transmits only those Bloch states that have symmetry matching to the low-decay-rate evanescent states in the barrier [19,20]. This process may significantly enhance TMR if the barrier selects conduction channels with a high degree of spin polarization (Fig. 2f). For example, the matching of the majority-spin Δ_1 band in the Fe (001) electrode to the Δ_1 evanescent state in the MgO (001) barrier is responsible for a large positive spin polarization and giant values of TMR predicted [20, 21] and observed [22, 23] in crystalline Fe/MgO/Fe (001) MTJs.

3. AFMTJs with collinear AFM electrodes

A vanishing net magnetization of antiferromagnets (Figs. 3a and 3b) makes the realization of TMR in AFMTJs much more challenging. AFMTJs represent tunnel junctions with two AFM electrodes whose Néel vector can be aligned parallel (P) or antiparallel (AP) resulting in the TMR effect (Fig. 3c). Various approaches have been theoretically proposed to observe TMR in AFMTJs, such as utilizing the quantum coherence between the staggered spin densities in AFM electrodes or between two uncompensated interfaces [24-29]. These effects, however, are not robust against interface roughness and disorder [30,31], and likely because of these reasons have not been confirmed in experiment. Recently, it has been predicted that some collinear antiferromagnets can exhibit momentum-dependent [32-41] and sublattice-dependent [11] transport spin polarization, even in the absence of spin-orbit coupling (SOC). These collinear antiferromagnets appear to be promising materials to serve as electrodes in AFMTJs [6,8,11].

TMR due to momentum-dependent spin polarization An antiferromagnet is a magnetically ordered material with equivalent magnetic moments exactly compensated, and thus zero net spontaneous magnetization [42, 43]. In collinear antiferromagnets with two antiparallel aligned magnetic sublattices, there exists a symmetry \hat{O} enforcing $\mathbf{m}_A = -\mathbf{m}_B$, where \mathbf{m}_α is the magnetization on magnetic sublattice $\alpha = A, B$ (Figs. 3a and 3b). The Néel vector $\mathbf{n} = \mathbf{m}_A - \mathbf{m}_B$ can serve as the magnetic order parameter. The most common \hat{O} symmetry is $\hat{P}\hat{T}$ that combines space inversion \hat{P} and time reversal \hat{T} (Fig. 3a). This symmetry enforces Kramers' spin degeneracy in the band structure, as $\hat{P}\hat{T}E_n^\uparrow(\mathbf{k}) = E_n^\downarrow(\mathbf{k})$ (Fig. 3a). This spin degeneracy also appears in compensated antiferromagnets with $\hat{O} = \hat{U}\hat{t}$ symmetry (\hat{U} is spin rotation and \hat{t} is half a unit cell translation) in the absence of SOC. As a result, the spin polarization p_{\parallel} of all conduction channels vanishes (Fig. 3a).

The magnetization compensation in an antiferromagnet can also be ensured by symmetries other than $\hat{P}\hat{T}$ and $\hat{U}\hat{t}$. Mirror/glide planes and rotation/screw axes in a crystal can also enforce $\mathbf{m}_A = -\mathbf{m}_B$. In such compensated antiferromagnet with $\hat{P}\hat{T}$ and $\hat{U}\hat{t}$ symmetries broken, spin splitting of the band

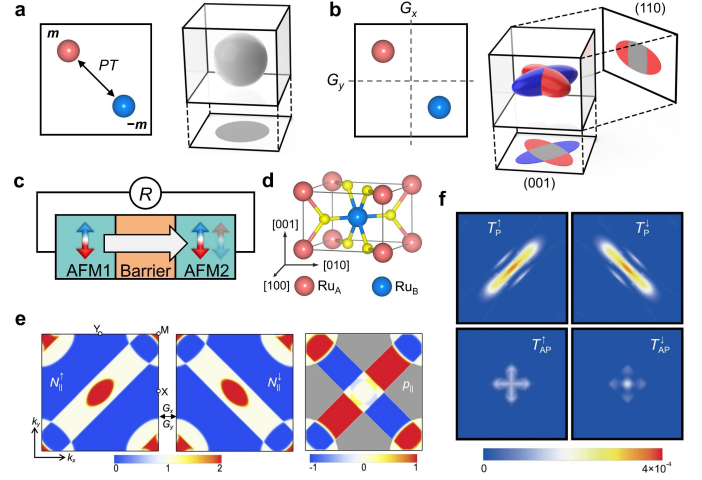


FIG. 3 (a) Schematics of the magnetic structure and the Fermi surface of a collinear antiferromagnet with magnetization compensated by $\hat{P}\hat{T}$ symmetry. The symmetry enforces spin degeneracy of the Fermi surface and conduction channels (indicated by grey color). (b) Schematics of the magnetic structure and the Fermi surface of a collinear antiferromagnet with magnetization compensated by two glide symmetries \hat{G}_x and \hat{G}_y . The symmetries allow spin splitting at wavevectors away from the \hat{G}_x and \hat{G}_y invariant planes (indicated by red and blue colors). This leads to the momentum-dependent spin polarization that is compensated in the (001) plane and uncompensated in the (110) plane. (c) Schematic of an AFMTJ with two AFM electrodes and a nonmagnetic tunnel barrier. (d) The atomic structure of a collinear AFM RuO_2 , which hosts two sublattices Ru_A and Ru_B with antiparallel magnetic moments. (e) Momentum-dependent conduction channels and associated spin polarizations in the 2D Brillouin zone of RuO_2 (001). (f) Calculated momentum-dependent transmission of a $\text{RuO}_2/\text{TiO}_2/\text{RuO}_2$ (001) AFMTJ. Figures (c-f) are reprinted from Ref. [6] under permission of the Creative Commons CC BY license.

structure appears even in the absence of SOC. This subgroup of antiferromagnets was dubbed as “altermagnets” [39,40] and their spin-split electronic structure was well understood based on the symmetry analyses [32-41]. Particularly, the spin point/space group theories [44,45] provide powerful tools to understand the nonrelativistic properties of magnets and their relation to spintronics [38,39, 46-49].

Figure 3b shows a typical spin-split Fermi surface of an altermagnet. Here, although $\hat{P}\hat{T}$ and $\hat{U}\hat{t}$ symmetries are broken, there are two glide symmetries, \hat{G}_x and \hat{G}_y , that connect two sublattices. The Fermi surface exhibits an anisotropic spin distribution $s(\mathbf{k})$ that is \hat{T} -odd, i.e. $s(\mathbf{k}) = s(-\mathbf{k})$. This contrasts with a \hat{T} -even spin distribution in SOC-split non-magnets, where $s(\mathbf{k}) = -s(-\mathbf{k})$. The anisotropic \hat{T} -odd $s(\mathbf{k})$ makes transport properties direction dependent. For example, in the [001] transport direction, the \mathbf{k}_{\parallel} -dependent conduction channels in the (001) 2D Brillouin zone host antisymmetric spin polarizations, i.e. $p_{\parallel}(k_x, k_y) = -p_{\parallel}(k_x, -k_y) = -p_{\parallel}(-k_x, k_y)$,

due to the [001] direction being invariant under \hat{G}_x and \hat{G}_y . As a result, a current flowing along the [001] direction is globally spin neutral [6]. On the contrary, an uncompensated p_{\parallel} appears in the conduction channels in the (110) 2D Brillouin zone, due to the [110] direction not being invariant under \hat{G}_x and \hat{G}_y . This allows a net spin-polarized current along the [110] direction with a finite transport spin polarization p (Fig. 3b) [50, 51].

Due to TMR being controlled by the \mathbf{k}_{\parallel} -dependent spin polarization p_{\parallel} , even for the transport direction supporting only spin-neutral currents ($p = 0$), altermagnets can produce TMR in AFMTJs. This possibility has been investigated for RuO₂ [6], a high-temperature AFM metal discovered recently [52, 53]. RuO₂ has a rutile structure with two magnetic sublattices Ru_A and Ru_B (Fig. 3d). Its magnetic space group $P4_2'/mnm'$ ensures the compensated magnetization and spin-split electronic structure. The RuO₂ Fermi surface has similar characteristics to those shown in Fig. 3b. In the (001) stacking, the conduction channels reveal an antisymmetric distribution of p_{\parallel} with respect to the \hat{G}_x and \hat{G}_y planes in the 2D Brillouin zone (Fig. 3e). Since switching the AFM Néel vector reverses p_{\parallel} , matching p_{\parallel} in a RuO₂ (001)-based AFMTJ can be controlled by the relative orientation of the Néel vector in the two electrodes. This ensures a finite TMR. First-principles quantum-transport calculations for all-rutile RuO₂/TiO₂/RuO₂ (001) AFMTJs confirm this prediction [6]. As seen from Fig. 3f, the distribution of T_{\parallel}^{σ} in the P state echoes the distribution of N_{\parallel}^{σ} in bulk RuO₂ (001), while T_{\parallel}^{σ} in the AP state is blocked at the wavevectors with $|p_{\parallel}| = 1$ in bulk RuO₂ (001). The resulting TMR is $\sim 500\%$ which is comparable to the TMR predicted for conventional Fe/MgO/Fe MTJs [20,21].

A giant TMR also appears in a RuO₂/TiO₂/RuO₂ (110) AFMTJ, where p_{\parallel} is uncompensated in the RuO₂ (110) 2D Brillouin zone supporting a spin-polarized current with a finite p [51]. While in this case, TMR is expected directly from the presence of the net spin polarization p of RuO₂ (110) (like in a FM MTJ), this conventional contribution to TMR appears to be small compared to the contribution associated with the matching of \mathbf{k}_{\parallel} -dependent spin polarization p_{\parallel} in the two electrodes.

Altermagnets such as RuO₂ (110) can also serve as a counter electrode in MTJs with a single FM electrode. Since both FM and AFM electrodes have finite and uncompensated p_{\parallel} , the TMR is expected to occur due to the p_{\parallel} matching mechanism. This approach can be used to verify the application potential of altermagnets, since FM electrodes can be easily switched by an applied magnetic field. From the practical perspective, this can also simplify the design of a conventional MTJ, due to no need for an additional pinning layer. The giant TMR of RuO₂/TiO₂/CrO₂ (110) all-rutile MTJ has been predicted recently [54,55], using half-metallic CrO₂ [56,57] as a FM electrode and RuO₂ as an AFM counter electrode.

TMR due to Néel spin currents In addition to the momentum-dependent spin polarization, the sublattice-dependent spin

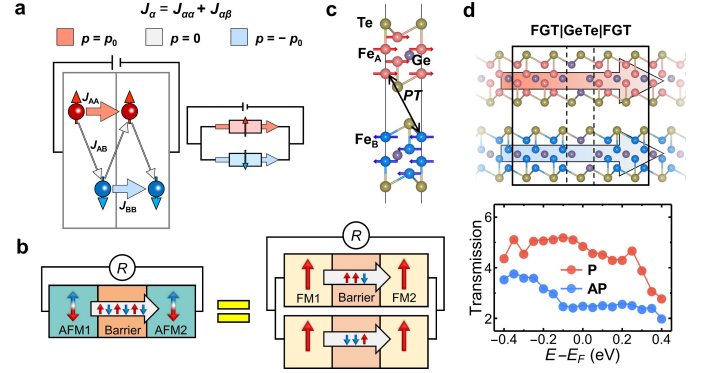


FIG. 4 (a) Schematics of staggered Néel spin currents in a collinear antiferromagnet with strong intra-sublattice coupling. (b) AFMTJ with Néel spin currents that can be qualitatively considered as two MTJs connected in parallel. (c) $\hat{P}\hat{T}$ symmetric 2D A-type AFM metal Fe₄GeTe₂ that supports Néel spin currents. (d) Lateral AFMTJ with sizable TMR despite the spin-degenerate electronic structure of Fe₄GeTe₂ electrodes. The figures are reprinted from Ref. [11] with permission.

polarization in real space can also result in TMR in collinear AFMTJs [11]. In a collinear AFM metal with two magnetic sublattices \mathbf{m}_A and \mathbf{m}_B , a longitudinal charge current J can be decomposed into intra-sublattice current $J_{\alpha\alpha}$ ($\alpha = A, B$) and inter-sublattice current $J_{\alpha\beta}$ ($\alpha \neq \beta$) (Fig. 4a), such that

$$J_{\alpha\beta} = J_{\alpha\beta}^{\uparrow} + J_{\alpha\beta}^{\downarrow}. \quad (5)$$

The associated spin current $J_{\alpha\beta}^s$ is

$$J_{\alpha\beta}^s = J_{\alpha\beta}^{\uparrow} - J_{\alpha\beta}^{\downarrow}. \quad (6)$$

The spin current flowing through sublattice α , dubbed the Néel spin current, I given by

$$J_{\alpha}^s = \sum_{\beta} J_{\alpha\beta}^s. \quad (7)$$

It hosts a sublattice-dependent spin polarization

$$p_{\alpha} = \frac{\sum_{\beta} J_{\alpha\beta}^s}{\sum_{\beta} J_{\alpha\beta}}. \quad (8)$$

The intra- and inter-sublattice currents are determined by the inter- and intra-sublattice electron hopping along the transport direction. Since the intra-sublattice currents J_{AA} and J_{BB} are spin-polarized, the Néel spin currents with large p_{α} can emerge if the intra-sublattice hopping is dominant.

For A-type antiferromagnets composed of antiparallel-aligned FM layers and C-type antiferromagnets composed of antiparallel-aligned chains, the intra-sublattice electron hopping is usually stronger than the inter-sublattice hopping. In these cases, the two AFM sublattices can be considered as connected in parallel with staggered Néel spin currents on the sublattices (Fig. 4a). AFMTJs based on such AFM electrodes can then be

qualitatively considered as two MTJs connected in parallel, which naturally supports TMR (Fig. 4b).

The Néel spin currents do not rely on spin-split electronic structure, and hence can emerge even in $\hat{P}\hat{T}$ symmetric antiferromagnets with Kramers' spin degeneracy. For example, in the recently discovered two-dimensional (2D) van der Waals magnet Fe_4GeTe_2 (Fig. 4c), where the AFM order is induced by doping [58], Néel spin currents with a large spin polarization $|p_\alpha| = 68\%$ for each layer are predicted, despite the spin-degenerate band structure (Fig. 4d), resulting in a sizable TMR in a Fe_4GeTe_2 -based AFMTJ (Fig. 4e) [11]. Such a lateral junction can be realized experimentally using the recently developed edge-epitaxy technique [59-61].

The TMR in the $\text{RuO}_2/\text{TiO}_2/\text{RuO}_2$ (001) AFMTJ discussed above can be also understood in terms of the Néel spin currents [11]. This is due to rutile MO_2 (M is a transition metal element) being composed of edge-sharing MO_6 octahedra chains along the [001] direction, where the adjacent chains share common corners of the octahedra. Therefore, RuO_2 can be regarded as a C-type antiferromagnet that supports Néel spin currents with a non-zero spin polarization. This fact has been verified for a $\text{RuO}_2/\text{TiO}_2/[\text{TiO}_2/\text{CrO}_2]_n/\text{CrO}_2$ (001) MTJ, where $[\text{TiO}_2/\text{CrO}_2]_n$ represents a multilayer of alternating TiO_2 (001) and CrO_2 (001) monolayers with n repeats [54]. The latter can be fabricated using modern thin-film growth techniques [62,63]. Although p_\parallel matching of bulk RuO_2 (001) and CrO_2 (001) electrodes is unable to generate TMR by symmetry, the presence of the $[\text{TiO}_2/\text{CrO}_2]_n$ multilayer results in a different effective barrier thickness for the Néel spin currents flowing on Ru_A and Ru_B sublattices. As a result, this AFMTJ can be decomposed into two parallel-connected MTJs with different barrier thickness, where conduction is dominated by the MTJ with smaller barrier thickness. This generates sizable TMR and proves the existence of the Néel spin currents [54].

4. AFMTJs with noncollinear AFM electrodes

In a magnetically frustrated crystal structure, collinear magnetic moment alignment may not guarantee the lowest energy. For example, in a Kagome lattice with AFM nearest-neighbor exchange interactions, the co-planar moments form a noncollinear AFM alignment with a 120° angle between each other (Fig. 5a). The Néel vector for such antiferromagnets is not uniquely defined, and the noncollinear AFM order is often represented by a magnetic multipole, a magnetic toroidal multipole [64], or even by direction of a small net magnetization generated by magnetic moment canting due to SOC [65,66]. The latter allows these noncollinear antiferromagnets to be considered as weak ferromagnets exhibiting spin-dependent transport properties, such as the anomalous Hall effect [67-69]. This fact has stimulated broad interest in the properties of noncollinear antiferromagnets.

Spin polarization in noncollinear antiferromagnets

Noncollinear antiferromagnets exhibit lower symmetry compared to their collinear counterparts. As a result, they generally support nonrelativistic spin-split band structures and spin-textured Fermi surfaces (Fig. 5b) [70, 71, 72], even in the presence of $\hat{U}\hat{t}$ symmetry [47]. Different from \hat{T} -even spin textures in nonmagnetic materials induced by SOC, the \hat{T} -odd spin textures support longitudinal spin-polarized currents [70, 73], indicating the possibility of using them as electrodes in AFMTJs (Fig. 5c).

However, since spin is not a good quantum number in noncollinear antiferromagnets, it is not clear if the spin-matching mechanism is still valid for noncollinear AFMTJs. The definition of p_\parallel given by Eq. (3) is inappropriate in this case. One can redefine the \mathbf{k}_\parallel -dependent spin polarization as a vector [74]

$$\mathbf{p}_\parallel(\mathbf{k}_\parallel) = \frac{\mathbf{s}_\parallel}{\sum_n |\mathbf{s}_{\parallel,n}|}, \quad (9)$$

where $\mathbf{s}_{\parallel,n}$ is the spin expectation value for band n at \mathbf{k}_\parallel and E_F , and $\mathbf{s}_{\parallel,i}$ is the net spin $\mathbf{s}_\parallel = \sum_n \mathbf{s}_{\parallel,n}$ at \mathbf{k}_\parallel . This definition is equivalent to Eq. (3) for the collinear case. For noncollinear magnets, although the magnitudes and orientations of \mathbf{s}_\parallel vary with \mathbf{k}_\parallel , the magnitude of spin polarization $p_\parallel = |\mathbf{p}_\parallel|$ is large when spins $\mathbf{s}_{\parallel,n}$ at \mathbf{k}_\parallel are nearly parallel in all conduction channels n , and is exactly 100% when only one conduction channel is present. Therefore, for noncollinear AFMTJs with two identical electrodes, the spin matching mechanism is expected to work if p_\parallel is large [74].

TMR in noncollinear AFMTJs The possibility of TMR in noncollinear AFMTJs has been proposed based on the predicted transport spin polarizations of Mn_3X ($X = \text{Sn}$ and Ir) [70] and ANMn_3 ($A = \text{Ga}, \text{Ni}, \text{Sn}, \text{or Pt}$) [73], and then calculated from first principles for AFMTJs with noncollinear AFM Mn_3Sn electrodes [7]. Mn_3Sn has a hexagonal D0_{19} structure of space group $P6_3/\text{mmc}$, where Mn atoms form a Kagome-type frustrated lattice, with the magnetic moments aligned with 120° angles between each other [66] (Fig. 5d). Such a magnetic alignment belongs to a magnetic space group $\text{Cmc}'m'$ that has $\hat{P}\hat{T}$ and $\hat{U}\hat{t}$ symmetries broken. This results in a non-spin-degenerate electronic structure with three Fermi surface sheets, each having finite momentum-dependent spin expectation values. Figure 5e shows the spin texture contributed by one of these sheets, indicating a finite \mathbf{p}_\parallel and thus a possibility for Mn_3Sn to serve as electrodes in a noncollinear AFMTJ. There are three other equivalent magnetic states in Mn_3Sn , which can be obtained by a 60° rotation around the [001] axis. Switching between these magnetic alignments in one Mn_3Sn electrode while keeping the other fixed in a $\text{Mn}_3\text{Sn}/\text{vacuum}/\text{Mn}_3\text{Sn}$ AFMTJ changes the matching conditions for \mathbf{p}_\parallel and generates sizable TMR as large as $\sim 300\%$ (Fig. 5f) [7]. A large TMR has

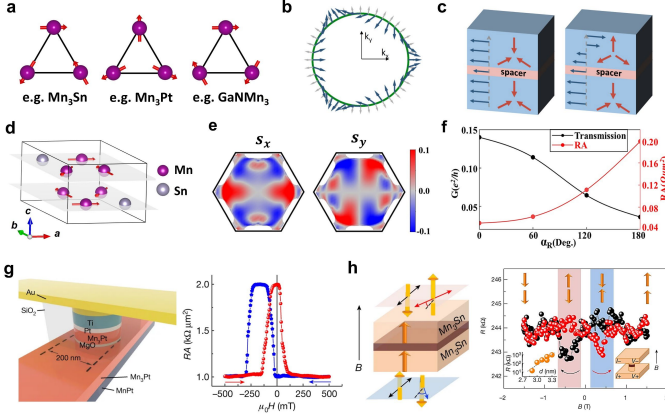


FIG. 5 (a) Schematic of the typical noncollinear AFM alignments. (b) Non-relativistic anisotropic spin texture at the Fermi surface of a noncollinear antiferromagnet supporting spin-polarized currents. (c) Schematic of a noncollinear AFMTJ with P (left) and AP (right) Néel vectors. Figures (b) and (c) are reprinted from Ref. [70] with permission. (d) Atomic and magnetic structure of Mn₃Sn. (e) Projected to the (0001) plane spin distribution on a selected Fermi surface sheet in Mn₃Sn. (f) Calculated tunneling conductance G per lateral unit cell area (left axis) and resistance-area (RA) product (right axis) for a Mn₃Sn/vacuum/Mn₃Sn AFMTJ when the magnetic domain shown in (d) is rotated by an angle α_R around the [0001] axis. Figures (e,f) are reprinted from Ref. [7] with permission. (g,h) Experimental results on TMR in Mn₃Pt/MgO/Mn₃Pt (g) and Mn₃Sn/MgO/Mn₃Sn (h) tunnel junctions. Left panels schematically show geometry of the AFMTJs; right panels show resistance vs applied magnetic field. Figure (g) is reprinted from Ref. [9] with permission. Figure (h) is reprinted from Ref. [10] under permission of the Creative Commons CC BY license.

also been predicted for noncollinear AFMTJs based on Mn₃Pt [9] and GaNMn₃ [74] electrodes.

Unlike collinear antiferromagnets whose magnetic state is difficult to control by external stimuli (this is why collinear AFMTJs have not been experimentally realized yet), noncollinear antiferromagnets can be controlled by a magnetic field [66,75] or a spin torque [76-79]. This is due to nonvanishing net magnetization induced by SOC [66], strain [80], or interfaces [81]. Therefore, a noncollinear AFTMJ is easier to realize in experiment.

Recently, two independent experiments have been successfully performed to observe TMR in noncollinear AFMTJs [9, 10]. The first one [9] utilized cubic AFM Mn₃Pt as electrodes and MgO as barrier in this AFMTJ (Fig. 5g). The bottom Mn₃Pt (001) layer was pinned by the exchange bias from an adjacent collinear AFM MnPt layer, while the top Mn₃Pt layer was free to be switched by an external magnetic field. The maximum TMR in this AFMTJ was found to be about 100% at room temperature (Fig. 5g) and about 138% at 10 K. Several devices have been tested and more than 50% of them had room-temperature TMR of more than 70%.

Another work [10] studied noncollinear Mn₃Sn/MgO/Mn₃Sn AFMTJ (Fig. 5h), where the bottom epitaxial Mn₃Sn layer had a (0111) orientation, and the top Mn₃Sn layer was polycrystalline. The P and AP states in this AFMTJ could be switched by the magnetic field producing TMR of about 2% at room temperature (Fig. 5h). The effect appeared to be not as large as that predicted [7] likely due to polycrystallinity of the top magnetic layer.

5. Spin torques in AFMTJs

Although magnetic fields are widely used to toggle between P and AP states in MTJs, their generation requires substantial currents making them energy inefficient. For low-power and high-density applications, spin torques are more favorable and thus have been extensively explored [82-88]. The spin-torque control of magnetization is even more critical for AFMTJs, since most AFM electrodes (except those with SOC-induced small net magnetic moment), are insensitive to a magnetic field.

Spin torques for magnetic switching The dynamics of a magnet can be well described by the Landau-Lifshitz-Gilbert-Slonczewski equation [82,89]:

$$\dot{\mathbf{m}}_\alpha = -\gamma \mathbf{m}_\alpha \times \mathbf{H}_{eff,\alpha} + \alpha_G \mathbf{m}_\alpha \times \dot{\mathbf{m}}_\alpha + \boldsymbol{\tau}_\alpha^{FL} + \boldsymbol{\tau}_\alpha^{DL}, \quad (10)$$

where \mathbf{m}_α is the magnetization of sublattice α , α_G is the damping constant, γ is the gyromagnetic ratio. The first two terms in Eq. (10) describe the precession and damping torques induced by the intrinsic effective field $\mathbf{H}_{eff,\alpha}$. The two last terms are external field-like and damping-like spin torques $\boldsymbol{\tau}_\alpha^{FL} \propto -\mathbf{m}_\alpha \times \mathbf{p}_\alpha$ and $\boldsymbol{\tau}_\alpha^{DL} \propto -\mathbf{m}_\alpha \times (\mathbf{m}_\alpha \times \mathbf{p}_\alpha)$, where \mathbf{p}_α is the current induced non-equilibrium spin polarization on sublattice \mathbf{m}_α . For ferromagnets, $\mathbf{H}_{eff,\alpha}$ is mostly determined by the anisotropy field $\mathbf{H}_{K,\alpha}$, and spin torques driven by \mathbf{p}_α can directly compete with the intrinsic torques to switch magnetization. The switching of ferromagnets is therefore controlled by $\mathbf{H}_{K,\alpha}$ and occurs in the GHz frequency range.

In MTJs, spin polarization \mathbf{p}_α is carried by the longitudinal current flowing across the junction. The tunneling current emitted by one electrode carries spin angular momentum that can be transferred to the magnetic moment of the other electrode, generating a spin-transfer torque (STT) [84]. In addition, spin torques can be produced by an in-plane current via spin-Hall [87] and Rashba-Edelstein effects [85]. This requires an additional spin-source layer that is adjacent to the free layer and has a large SOC. This type of spin torque is known as the spin-orbit torque (SOT).

Spin torques in collinear AFM electrodes Switching antiferromagnets by spin torques is more complicated than switching ferromagnets [88,90-96]. For example, in a simple collinear antiferromagnet with two antiparallel sublattices ($\alpha = A, B$), $\mathbf{H}_{eff,\alpha}$ contains an additional exchange field $\mathbf{H}_{E,\alpha}$, which exerts exchange torques $\boldsymbol{\tau}_{E,\alpha}^F \propto -\mathbf{m}_\alpha \times \mathbf{H}_E$ and $\boldsymbol{\tau}_{E,\alpha}^D \propto -\mathbf{m}_\alpha \times$

$(\mathbf{m}_\alpha \times \mathbf{H}_{\text{eff},\alpha})$. Here, superscripts F and D denote the associated precession (field) and damping torques, respectively. Since $\mathbf{H}_{E,\alpha} \propto -\mathbf{m}_\beta$ ($\alpha \neq \beta$), $\boldsymbol{\tau}_{E,\alpha}^F$ and $\boldsymbol{\tau}_{E,\alpha}^D$ vanish if the two sublattices are antiparallel. However, if \mathbf{m}_α and \mathbf{m}_β are tilted due to a spin torque, the exchange field generates staggered $\boldsymbol{\tau}_{E,\alpha}^F$. Due to $\mathbf{H}_{E,\alpha}$ being typically a factor of 10^3 greater than $\mathbf{H}_{K,\alpha}$, it is practically impossible to create such a large spin torque to directly compete with $\boldsymbol{\tau}_{E,\alpha}^F$ for switching the Néel vector. However, the spin torque can be used to tilt \mathbf{m}_α and \mathbf{m}_β enforcing a Néel vector precession driven by $\boldsymbol{\tau}_{E,\alpha}^F$ [90]. Due to the large $\mathbf{H}_{E,\alpha}$, such precession occurs in the THz frequency range. This property can be used for the switching of the Néel vector, provided that an appropriate torque can be generated.

We, first, consider a damping-like torque that is usually employed to switch ferromagnets and can be generated by a uniform spin polarization \mathbf{p} of a tunneling current, a spin-Hall effect, or a Rashba-Edelstein effect [82-88]. Normally, in collinear antiferromagnets, these effects lead to $\mathbf{p}_A = \mathbf{p}_B = \mathbf{p}$ for the two sublattices, which results in a uniform damping-like torque $\boldsymbol{\tau}_A^{DL} = \boldsymbol{\tau}_B^{DL}$ and staggered field-like torque $\boldsymbol{\tau}_A^{FL} = -\boldsymbol{\tau}_B^{FL}$.

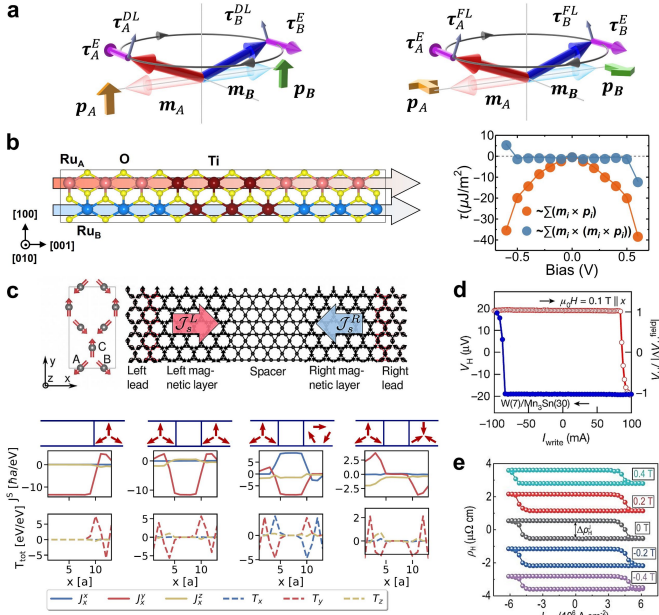


FIG. 6 (a) Schematics of the dynamics of collinear antiferromagnets induced by a spin current with uniform spin polarizations (left) and staggered spin polarizations (right) on two sublattices. (b) Atomic structure of a RuO₂/TiO₂/RuO₂ (001) AFMTJ (left) and calculated STT driven by Néel spin currents in this AFMTJ (right). Reprinted from Ref. [11] with permission. (c) Schematic noncollinear AFMTJ (top) and calculated STT in this AFMTJ for different magnetic states of the electrodes (bottom). Reprinted from Ref. [96] with permission. (d) SOT switching of an epitaxial Mn₃Sn film with assistance of a magnetic field. Reprinted from Ref. [77] with permission. (e) Field-free spin-torque switching of a Mn₃Sn polycrystalline film. Reprinted from Ref. [79] under permission of the Creative Commons CC BY license.

The former tilts \mathbf{m}_A and \mathbf{m}_B causing the staggered $\boldsymbol{\tau}_{E,\alpha}^F$ to drive an ultrafast oscillation of the Néel vector in the plane perpendicular to \mathbf{p} (Fig. 6a, left). This oscillation is persistent that is promising for THz applications [90]. However, the damping-like spin torque induced by a uniform polarization \mathbf{p} is *indeterministic* for the reversal of the Néel vector.

We note, however, that such spin torque can be used to rotate the Néel vector between the easy axes in antiferromagnets with multi-axial anisotropy. For example, in an antiferromagnet with bi-axial anisotropy and easy axes along the x and y directions, the Néel vector can be switched from the initial x direction to the final y (or $-y$) direction. This is because a current-induced uniform \mathbf{p} along the x axis exerts a damping-like spin torque that drives a persistent oscillation confined within the y - z plane. When the current is released, the Néel vector relaxes to the easy y axis. This approach has been employed in heterostructures of antiferromagnet/heavy metal bilayers, where \mathbf{p} was generated by the spin Hall effect in the heavy metal layers [95,97-99].

In contrast, if a staggered spin polarization is induced in an antiferromagnet, i.e. $\mathbf{p}_A = -\mathbf{p}_B$, the staggered damping-like torque $\boldsymbol{\tau}_A^{DL} = -\boldsymbol{\tau}_B^{DL}$ and the uniform field-like torque $\boldsymbol{\tau}_A^{FL} = \boldsymbol{\tau}_B^{FL}$ can be generated [93,94]. The latter tilts \mathbf{m}_A and \mathbf{m}_B , resulting in the staggered $\boldsymbol{\tau}_{E,\alpha}^F$ that drives the rotation of \mathbf{m}_α toward the direction of \mathbf{p}_α (Fig. 6a, right). When \mathbf{m}_α is rotated to be parallel to \mathbf{p}_α , $\boldsymbol{\tau}_\alpha^{FL}$ vanishes and the dynamics of the Néel vector stops. Therefore, if the staggered \mathbf{p}_α is collinear to the easy axis of an antiferromagnet, the ultrafast and *deterministic* switching of the Néel vector can be achieved.

Previously, such a staggered \mathbf{p}_α and uniform $\boldsymbol{\tau}_\alpha^{FL}$ have been considered in AFMTJs based on quantum coherence between the staggered spin densities in the AFM electrodes or between two interfaces [24-29]. These effects, however, are not robust against disorder and suffer strong spin dephasing [29-31]. It was found that $\hat{P}\hat{T}$ -symmetric antiferromagnets can support staggered \mathbf{p}_α via the Rashba-Edelstein effect [93,94], provided that the sublattices in such antiferromagnets are locally non-centrosymmetric [100,101]. This generates the Néel SOTs that have been confirmed experimentally [94, 102]. However, antiferromagnets with this property, such as CuMnAs [94], Mn₂Au [93,102], and MnPd₂ [103], support neither the momentum-dependent spin polarizations nor notable Néel spin currents, and thus are not suitable to serve as electrodes in AFMTJs.

The required staggered \mathbf{p}_α and uniform $\boldsymbol{\tau}_\alpha^{FL}$ can be realized in AFMTJs due to the Néel spin currents. Tunneling Néel spin currents can transfer the staggered \mathbf{p}_α from the reference layer to the free layer, exerting the required torques for switching. First-principles quantum-transport calculations have been performed for RuO₂/TiO₂/RuO₂ (001) AFMTJs (Fig. 6b) and Fe₄GeTe₂/vacuum/Fe₄GeTe₂ lateral AFMTJs [11]. These calculations show that the total field-like torque in the free layer

is large, while the total damping-like torque is small, consistent with the expectation of $\tau_A^{FL} = \tau_B^{FL}$ and $\tau_A^{DL} = -\tau_B^{DL}$. The total field-like torque induced by the Néel spin currents is comparable to that in a Fe/MgO/Fe MTJ with similar barrier thickness [104], robust to the interface structure, and thus can be used to generate the ultrafast deterministic switching of the Néel vector in AFMTJs [11].

Spin torques in noncollinear AFM electrodes. In a noncollinear antiferromagnet with three magnetic sublattices (\mathbf{m}_A , \mathbf{m}_B , and \mathbf{m}_C) aligned within the Kagome plane, the spin-torque dynamics exhibits rich behavior. For example, when an external spin current is injected into a noncollinear antiferromagnet and its spin polarization \mathbf{p} is perpendicular to the Kagome plane, i.e. $\mathbf{p} \perp \mathbf{m}_\alpha$, the damping-like torque τ_α^{DL} is uniform. This torque tilts \mathbf{m}_α along the out-of-plane direction, causing the finite $\tau_{E,\alpha}^F$ to drive an ultrafast oscillation of \mathbf{m}_α within the Kagome plane (like in the case of Fig. 6a, left) [105,106]. In the presence of multi-domain states, such \mathbf{p} may drive fast motion of domain walls [107].

If \mathbf{p} is in the plane, the resulting torques on the sublattices are different, due to different directions of \mathbf{m}_α relative to \mathbf{p} . For example, in a noncollinear AFMTJ based on a Mn₃Pt-type electrode (Fig. 6c) [96], the magnetic group symmetry allows an x -directional longitudinal spin current carrying spin polarization along the y direction, i.e. $\mathbf{p} \parallel \mathbf{m}_C$ [70]. Theoretical modeling shows that this spin current exerts damping-like self-torques on \mathbf{m}_A and \mathbf{m}_B (Fig. 6c, bottom) [96]. Such self-torques, though interesting, are not able to switch a noncollinear antiferromagnet, because they are internally generated within the antiferromagnet and rotated together with its magnetic order. In contrast, STTs generated by a tunneling spin current injected from another noncollinear AFM electrode can perform the deterministic switching (Fig. 6c, bottom). The self-torques in this case can be useful to reduce the switching current density [96].

Besides the global spin currents, noncollinear local spin currents due to nonrelativistic [96] and relativistic [108] origins can also emerge in noncollinear antiferromagnets. In addition, noncollinear antiferromagnets support the nonrelativistic Rashba-Edelstein effect [109]. These factors can also contribute to spin torques. Furthermore, due to the existence of the nonrelativistic net magnetization [66], many noncollinear antiferromagnets can be considered as weak ferromagnets, and their spin-torque dynamics can be understood as the interplay of weak magnetization and current-induced spin polarization. For example, in an epitaxial noncollinear AFM Mn₃Sn with perpendicular net magnetization, SOT switching by a spin Hall current generated from an adjacent heavy metal layer requires an assisting in-plane magnetic field (Fig. 6d) [76-78]. This is like the conventional SOT switching of a perpendicular ferromagnet. Remarkably, a field-free switching of a polycrystalline Mn₃Sn film (Fig. 6e) has been reported recently [79], which may combine the different types of spin torques mentioned above.

Finally, we note that STTs in noncollinear AFMTJs are different from those in collinear MTJs [96,110]. The latter cannot occur for the perfect P or AP states, and hence thermal activation is required to induce magnetic fluctuations and activate switching. In a noncollinear AFMTJ, however, STTs can occur in any configuration due to noncollinear sublattice moments (Fig. 6c, bottom) [96]. This eliminates the requirement of thermal activation that suffers from energy dissipation.

6. Summary and Outlook

As is evident from this brief review, AFMTJs exhibit interesting functional properties useful for applications. The most notable among them is the giant TMR effect. In conjunction with the possibility of the AFM Néel vector switching by spin torques, it provides potential for novel and more advanced AFM-RAMs. The underlying physics of these properties is determined by the strong exchange interactions in AFM metals, crystal symmetry of the antiferromagnets, and the associated nonrelativistic momentum- and sublattice-dependent spin polarizations. Due to the strong magnetoresistive responses, AFMTJs are expected to be superior to those AFM spintronic devices that are controlled by the relativistically-induced spin-dependent properties associated with a weak SOC [94,95,97,111-113]. However, while AFMTJs have promising perspectives, their investigations are still in a rudimentary stage of development, and thus substantial efforts are required to further elucidate their basic properties and evaluate their value for spintronics.

Although the mechanism of TMR in collinear AFMTJs has been understood, experimental demonstrations are still lacking. This is largely due to difficulties of controlling the Néel vector in collinear antiferromagnets. In this regard, an MTJ with a single FM electrode and an AFM counter electrode can be employed as a preliminary test for using collinear antiferromagnets in AFMTJs [54,55]. In addition, as-grown AFM films usually host a complex domain structure with oppositely aligned AFM domains. Using such films as a reference layer in an AFMTJ would obviously diminish TMR. This problem could be addressed by depositing an AFM film on a FM layer, so that the AFM domains are aligned and switched by an exchange bias [114,115]. Once the domains in the AFM reference layer are well aligned, the Néel vector of the free AFM layer could be deterministically switched by spin torques induced by the Néel spin currents [11].

Ultimately, it is desirable to use electric means to align the collinear AFM domains rather than a magnetic field-controlled exchange bias. Although a spin current with a uniform spin polarization cannot deterministically switch the Néel vector in collinear antiferromagnets on its own, this may be possible with assistance of other factors, such as an external magnetic field, a Dzyaloshinskii-Moriya interaction [116,117], or interfacial uncompensated magnetization. These possibilities are worth further investigations. In addition, in an X-type antiferromagnet, aligning AFM domains is possible by passing an external spin

current that exerts a spin torque on a single magnetic sublattice [118]. A similar approach is feasible for AFMTJs with an engineered structure, such as $\text{RuO}_2/\text{TiO}_2/[\text{TiO}_2/\text{CrO}_2]_n/\text{CrO}_2(001)$ [54].

Spin-torque switching of noncollinear AFM metals have been demonstrated in several experiments [76-79], but requires further investigations. There are various mechanisms to induce spin polarization globally and/or locally in noncollinear antiferromagnets, and various factors affecting its magnitude and direction. Due to relatively low symmetry of noncollinear antiferromagnets, the spin-polarization magnitude is expected to strongly depend on the electric field direction causing dissimilar spin-torque dynamics of noncollinear antiferromagnets with different crystallographic orientations. Net magnetization due to relativistic spin canting [65,66], piezomagnetism [80], and breaking periodicity at the interface [81] may also influence the spin-torque dynamics.

We expect that spin-torque switching of antiferromagnets could be very energy-efficient. To switch the Néel vector, the applied spin torque does not need to directly compete with the strong exchange field, but rather with much smaller magnetic anisotropy and intrinsic damping. Only a slight tilting of the magnetic moments by the spin torque is required to initiate the exchange-driven spin dynamics. Therefore, the associated critical current is expected to be comparable or smaller than that needed for the spin-torque switching of ferromagnets. In addition, the spin-torque switching of antiferromagnets is expected to be much faster than that of ferromagnets. As a result, the comparable or smaller switching current and the much shorter switching time are expected to consume much less energy.

In addition to the spin torque, there are other means to switch the Neel vector in antiferromagnets. For example, it is possible to control the Néel vector by piezoelectric strain induced by electric field [119, 120]. In magnetoelectric antiferromagnets, such as BiFeO_3 [121,122,123] and Cr_2O_3 [124], may be potentially employed as an exchange-coupled under-(over-)layer in AFMTJs to control the Néel vector of the AFM electrode by an electric field applied to the magnetoelectric. The Néel vector may also be switched by voltage controlled magnetic anisotropy (VCMA) [125].

Another issue that needs to be addressed is the material choice for AFMTJs. Among the relatively small number of known altermagnets, only three of them [52,126,127], to the best of our knowledge, are metallic and antiferromagnetic at room temperature. This limits the choice of altermagnetic electrodes for realistic applications. Further material search and design are required [128,129]. In this regard, noncollinear antiferromagnets may be a better choice, because many of them have the Néel temperature above room temperature and two of them, namely Mn_3Pt and Mn_3Sn , have already demonstrated their functionality in AFMTJs [9,10]. An important issue which needs to be addressed is magnetic anisotropy which is typically much

weaker in noncollinear antiferromagnets than in their collinear counterparts. To realize robust nonvolatile states in noncollinear AFMTJs, optimizing their magnetic anisotropy is necessary. Yet, weak magnetic anisotropy makes noncollinear AFMTJs suitable for magnetic sensor applications [130].

AFMTJs with AFM electrodes that have multiple anisotropy axes may be useful to realize spintronic devices with multiple non-volatile resistance states. For example, in the case on Mn_3Sn , different non-volatile resistance states can be obtained associated with the ground-state Néel vector configurations of the AFM electrodes (Fig. 5f). As we have discussed in Sec. 4, switching between these states can be accomplished by a damping-like spin torque.

Tunneling barrier also plays a very important role in the performance of AFMTJs. The widely used MgO in conventional MTJs [22,23] may be not an optimal choice for AFMTJs [9,10]. This is due to the evanescent states in MgO mostly supporting transmission of electrons with the transverse wave vectors \mathbf{k}_\parallel around the center of the 2D Brillouin zone [20,21], where the spin polarization p_\parallel of the AFM electrodes may be relatively small [6,74]. It would be desirable to search for insulating materials with low decay rates at \mathbf{k}_\parallel away from the zone center to match the spin-polarized conduction channels of AFM electrodes when designing AFMTJs [74]. In addition, if the barrier exhibits a sizable SOC, interesting transport phenomena may occur in AFMTJs due to the interplay between the non-relativistic and relativistic effects, such as unconventional Hall effects [131-133], tunneling anisotropic magnetoresistance [134], and non-reciprocal transport [135].

Finally, probably the most critical requirement for observing the predicted giant TMR effects in AFMTJs is good crystallinity of AFMTJs. Conservation of the transverse momentum \mathbf{k}_\parallel in the process of tunneling imposes stringent conditions on the quality of thin films and heterostructures comprising AFMTJs. Since the momentum- and sublattice-dependent spin polarization in antiferromagnets is highly anisotropic, capabilities for epitaxial growth of AFMTJs along selected directions are required. These challenges need to be addressed by qualified material scientists.

Overall, there are clear indications that AFMTJs can overperform conventional MTJs in terms of the TMR magnitude, switching speed, and packing density. The predicted TMR values are gigantic, and the first experimental data provides a lot of optimism. The switching speed of AFMTJs is expected to be a few orders in magnitude faster. The high packing density is guaranteed by the absence of stray magnetic fields. Thus, AFMTJs have potential to become a new standard for spintronic devices, making this research field rich with opportunities for innovation and new developments.

Acknowledgments

The authors thank Shui-Sen Zhang and Yuan-Yuan Jiang for their help in preparing figures. This work was supported by the

National Science Foundation through DMR (NSF grant No. DMR-2316665) and EPSCoR RII Track-1 (NSF grant OIA-2044049) programs. D.F.S. acknowledges support from the National Key R&D Program of China (Grant No. 2021YFA1600200), the National Natural Science Foundation of

China (Grants Nos. 12274411, 12241405, and 52250418), the Basic Research Program of the Chinese Academy of Sciences Based on Major Scientific Infrastructures (Grant No. JZHKYPT-2021-08), and the CAS Project for Young Scientists in Basic Research (Grant No. YSBR-084).

- [1] E. Y. Tsymlal and I. Žutić, Eds., *Spintronics Handbook: Spin Transport and Magnetism*, 2-nd edition (CRC press, 2019).
- [2] T. Jungwirth, X. Marti, P. Wadley, and J. Wunderlich, Antiferromagnetic spintronics, *Nat. Nanotech.* **11**, 231 (2016).
- [3] V. Baltz, A. Manchon, M. Tsoi, T. Moriyama, T. Ono, and Y. Tserkovnyak, Antiferromagnetic spintronics, *Rev. Mod. Phys.* **90**, 015005 (2018).
- [4] D. Xiong, Y. Jiang, K. Shi, A. Du, Y. Yao, Z. Guo, D. Zhu, K. Cao, S. Peng, W. Cai, D. Zhu, and Weisheng Zhao, Antiferromagnetic spintronics: An overview and outlook, *Fundamental Research*, **2**, 522 (2022).
- [5] T. Jungwirth, J. Sinova, A. Manchon, X. Marti, J. Wunderlich, and C. Felser, The multiple directions of antiferromagnetic spintronics, *Nat. Phys.* **14**, 200 (2018).
- [6] D.-F. Shao, S. H. Zhang, M. Li, C. B. Eom, and E. Y. Tsymlal, Spin-neutral currents for spintronics, *Nat. Commun.* **12**, 7061 (2021).
- [7] J. Dong, X. Li, G. Gurung, M. Zhu, P. Zhang, F. Zheng, E. Y. Tsymlal, and J. Zhang, Tunneling magnetoresistance in noncollinear antiferromagnetic tunnel junctions, *Phys. Rev. Lett.* **128**, 197201 (2022).
- [8] L. Šmejkal, A. Birk Hellenes, R. González-Hernández, J. Sinova, and T. Jungwirth, Giant and tunneling magnetoresistance in unconventional collinear antiferromagnets with nonrelativistic spin-momentum coupling, *Phys. Rev. X* **12**, 011028 (2022).
- [9] P. Qin, H. Yan, X. Wang, H. Chen, Z. Meng, J. Dong, M. Zhu, J. Cai, Z. Feng, X. Zhou, L. Liu, T. Zhang, Z. Zeng, J. Zhang, C. Jiang, and Z. Liu, Room-temperature magnetoresistance in an all-antiferromagnetic tunnel junction, *Nature* **613**, 485 (2023).
- [10] X. Chen, T. Higo, K. Tanaka, T. Nomoto, H. Tsai, H. Idzuchi, M. Shiga, S. Sakamoto, R. Ando, H. Kosaki, T. Matsuo, D. Nishio-Hamane, R. Arita, S. Miwa, and S. Nakatsuji, Octupole-driven magnetoresistance in an antiferromagnetic tunnel junction, *Nature* **613**, 490 (2023).
- [11] D. F. Shao, Y. Y. Jiang, J. Ding, S. H. Zhang, Z. A. Wang, R. C. Xiao, G. Gurung, W. J. Lu, Y. P. Sun, and E. Y. Tsymlal, Neel spin currents in antiferromagnets, *Phys. Rev. Lett.* **130**, 216702 (2023).
- [12] M. Julliere, Tunneling between ferromagnetic films, *Phys. Lett.* **54A**, 225 (1975).
- [13] J. S. Moodera, L. R. Kinder, T. M. Wong, and R. Meservy, Large magnetoresistance at room temperature in ferromagnetic thin film tunnel junctions, *Phys. Rev. Lett.* **74**, 3273 (1995).
- [14] E. Y. Tsymlal, O. N. Mryasov, and P. R. LeClair, Spin-dependent tunneling in magnetic tunnel junctions, *J. Phys.: Condens. Matter* **15**, R109-R142 (2003).
- [15] K. D. Belashchenko, E. Y. Tsymlal, M. van Schilfgaarde, D. Stewart, I. I. Oleinik, and S. S. Jaswal, Effect of interface bonding on spin-dependent tunneling from the oxidized Co surface, *Phys. Rev. B* **69**, 174408 (2004).
- [16] R. Landauer, Spatial variation of currents and fields due to localized scatterers in metallic conduction, *IBM J. Res. Dev.* **32**, 306 (1988).
- [17] S. Datta, *Electronic Transport in Mesoscopic Systems* (Cambridge University Press, 1995).
- [18] K. M. Schep, P. J. Kelly, and G. E. W. Bauer, Ballistic transport and electronic structure, *Phys. Rev. B* **57**, 8907 (1998).
- [19] Ph. Mavropoulos, N. Papanikolaou, and P. H. Dederichs, Complex band structure and tunneling through ferromagnet/insulator/ferromagnet junctions, *Phys. Rev. Lett.* **85**, 1088 (2000).
- [20] W. H. Butler, X. G. Zhang, T. C. Schulthess, and J. M. MacLaren, Spin-dependent tunneling conductance of Fe|MgO|Fe sandwiches, *Phys. Rev. B* **63**, 054416 (2001).
- [21] J. Mathon and A. Umerski, Theory of tunneling magnetoresistance of an epitaxial Fe/MgO/Fe (001) junction, *Phys. Rev. B* **63**, 220403 (2001).
- [22] S. Yuasa, T. Nagahama, A. Fukushima, Y. Suzuki, and K. Ando, Giant room-temperature magnetoresistance in single-crystal Fe/MgO/Fe magnetic tunnel junctions, *Nat. Mater.* **3**, 868 (2004).
- [23] S. Parkin, C. Kaiser, A. Panchula, P. M. Rice, B. Hughes, M. Samant, and S. H. Yang, Giant tunnelling magnetoresistance at room temperature with MgO (100) tunnel barriers, *Nat. Mater.* **3**, 862 (2004).
- [24] A. S. Núñez, R. A. Duine, P. Haney, and A. H. MacDonald, Theory of spin torques and giant magnetoresistance in antiferromagnetic metals, *Phys. Rev. B* **73**, 214426 (2006).
- [25] P. M. Haney, D. Waldron, R. A. Duine, A. S. Núñez, H. Guo, and A. H. MacDonald, *Ab initio* giant magnetoresistance and current-induced torques in Cr/Au/Cr multilayers, *Phys. Rev. B* **75**, 174428 (2007).
- [26] Y. Xu, S. Wang, and K. Xia, Spin-transfer torques in antiferromagnetic metals from first principles, *Phys. Rev. Lett.* **100**, 226602 (2008).
- [27] P. Merodio, A. Kalitsov, H. Ba, V. Baltz, and M. Chshiev, Spin-dependent transport in antiferromagnetic tunnel junctions, *Appl. Phys. Lett.* **105**, 122403 (2014).
- [28] M. Stamenova, R. Mohebbi, J. Seyed-Yazdi, I. Rungger, and S. Sanvito, First-principles spin-transfer torque in CuMnA|GaP|CuMnAs junctions, *Phys. Rev. B* **95**, 060403 (2017).
- [29] H. Saidaoui, A. Manchon, and X. Waintal, Robust spin transfer torque in antiferromagnetic tunnel junctions, *Phys. Rev. B* **95**, 134424 (2017).
- [30] H. B. M. Saidaoui, A. Manchon, and X. Waintal, Spin transfer torque in antiferromagnetic spin valves: From clean to disordered regimes, *Phys. Rev. B* **89**, 174430 (2014).
- [31] A. Manchon, Spin diffusion and torques in disordered antiferromagnets, *J. Phys. Condens. Matter* **29**, 104002 (2017).

- [32] S. Hayami, Y. Yanagi, and H. Kusunose, Momentum-dependent spin splitting by collinear antiferromagnetic ordering, *J. Phys. Soc. Jpn.* **88**, 123702 (2019).
- [33] M. Naka, S. Hayami, H. Kusunose, Y. Yanagi, Y. Motome, and H. Seo, Spin current generation in organic antiferromagnets, *Nat. Commun.* **10**, 4305 (2019).
- [34] L.-D. Yuan, Z. Wang, J.-W. Luo, E. I. Rashba, and A. Zunger, Giant momentum-dependent spin splitting in centrosymmetric low-Z antiferromagnets, *Phys. Rev. B* **102**, 014422 (2020).
- [35] S. Hayami, Y. Yanagi, and H. Kusunose, Bottom-up design of spin-split and reshaped electronic band structures in antiferromagnets without spin-orbit coupling: Procedure on the basis of augmented multipoles, *Phys. Rev. B* **102**, 144441 (2020).
- [36] L.-D. Yuan, Z. Wang, J.-W. Luo, and A. Zunger, A. Prediction of low-Z collinear and noncollinear antiferromagnetic compounds having momentum-dependent spin splitting even without spin-orbit coupling, *Phys. Rev. Mater.* **5**, 014409 (2021).
- [37] H. Y. Ma, M. Hu, N. Li, J. Liu, W. Yao, J.-F. Jia, and J. Liu, Multifunctional antiferromagnetic materials with giant piezomagnetism and noncollinear spin current, *Nat. Commun.* **12**, 2846 (2021).
- [38] P. Liu, J. Li, J. Han, X. Wan, and Q. Liu, Spin-group symmetry in magnetic materials with negligible spin-orbit coupling, *Phys. Rev. X* **12**, 021016 (2022).
- [39] L. Šmejkal, J. Sinova, and T. Jungwirth, Beyond conventional ferromagnetism and antiferromagnetism: A phase with nonrelativistic spin and crystal rotation symmetry, *Phys. Rev. X* **12**, 031042 (2022).
- [40] L. Šmejkal, J. Sinova, and T. Jungwirth, Emerging research landscape of altermagnetism, *Phys. Rev. X* **12**, 040501 (2022).
- [41] L. Yuan and A. Zunger, Degeneracy removal of spin bands in collinear antiferromagnets with non-interconvertible spin-structure motif pair, *Adv. Mater.* **35**, 2211966 (2023).
- [42] L. Néel, Propriétés magnétiques du manganèse et du chrome en solution solide étendue, *J. Phys. radium* **3**, 160 (1932).
- [43] L. Néel, Antiferromagnetism and ferrimagnetism, *Proc. Phys. Soc. A* **65**, 869 (1952).
- [44] W. F. Brinkman and R. J. Elliott, Theory of spin-space groups, *Proc. R. Soc. Lond., Ser. A, Math. Phys. Eng. Sci.* **294**, 343 (1966).
- [45] D. B. Litvin, Spin point groups, *Acta. Crystallogr. A* **33**, 279 (1977).
- [46] Z. Xiao, J. Zhao, Y. Li, R. Shindou, and Z.-D. Song, Spin Space groups: Full classification and applications, *arXiv:2307.10364* (2023).
- [47] J. Ren, X. Chen, Y. Zhu, Y. Yu, A. Zhang, J. Li, Y. Liu, C. Li, and Q. Liu, Enumeration and representation of spin space groups, *arXiv:2307.10369* (2023).
- [48] Y. Jiang, Z. Song, T. Zhu, Z. Fang, H. Weng, Z.-X. Liu, J. Yang, and C. Fang, Enumeration of spin-space groups: Towards a complete description of symmetries of magnetic orders, *arXiv:2307.10371* (2023).
- [49] X. Chen, J. Ren, J. Li, Y. Liu, and Q. Liu, Spin Space Group Theory and Unconventional Magnons in Collinear Magnets, *arXiv:2307.12366* (2023).
- [50] R. González-Hernández, L. Šmejkal, K. Výborný, Y. Yahagi, J. Sinova, T. Jungwirth, and J. Železný, Efficient electrical spin-splitter based on non-relativistic collinear antiferromagnetism, *Phys. Rev. Lett.* **126**, 127701 (2021).
- [51] Y.-Y. Jiang, Z.-A. Wang, K. Samanta, S.-H. Zhang, R.-C. Xiao, W. J. Lu, Y. P. Sun, E. Y. Tsymbal, and D.-F. Shao, Prediction of giant tunneling magnetoresistance in RuO₂/TiO₂/RuO₂ (110) antiferromagnetic tunnel junctions, *Phys. Rev. B* **108**, 174439 (2023).
- [52] T. Berlijn, P. C. Snijders, O. Delaire, H.-D. Zhou, T. A. Maier, H.-B. Cao, S.-X. Chi, M. Matsuda, Y. Wang, M. R. Koehler, P. R. C. Kent, and H. H. Weitering, Itinerant antiferromagnetism in RuO₂, *Phys. Rev. Lett.* **118**, 077201 (2017).
- [53] K.-H. Ahn, A. Hariki, K.-W. Lee, and J. Kuneš, RuO₂ antiferromagnetism in as d-wave Pomeranchuk instability, *Phys. Rev. B* **99**, 184432 (2019).
- [54] K. Samanta, Y.-Y. Jiang, T. R. Paudel, D.-F. Shao, and E. Y. Tsymbal, Tunneling magnetoresistance in magnetic tunnel junctions with a single ferromagnetic electrode, *arXiv:2310.02139* (2023).
- [55] B. Chi, L. Jiang, Y. Zhu, G. Yu, C. Wan, J. Zhang, and X. Han, Altermagnetic tunnel junctions of RuO₂/TiO₂/CrO₂, *arXiv:2309.09561* (2023).
- [56] P. Porta, M. Marezio, J. P. Remeika, and P. D. Dernier, Chromium dioxide: High pressure synthesis and bond lengths, *Mater. Res. Bull.* **7**, 157 (1972).
- [57] R. A. de Groot, F. M. Mueller, P. G. van Engen, and K. H. J. Buschow, New class of materials: Half-metallic ferromagnets, *Phys. Rev. Lett.* **50**, 2024 (1983).
- [58] J. Seo, E. S. An, T. Park, S.-Y. Hwang, G.-Y. Kim, K. Song, W.-s. Noh, J. Y. Kim, G. S. Choi, M. Choi, E. Oh, K. Watanabe, T. Taniguchi, J. -H. Park, Y. J. Jo, H. W. Yeom, S.-Y. Choi, J. H. Shim, and J. S. Kim, Tunable high-temperature itinerant antiferromagnetism in a van der Waals magnet, *Nat. Commun.* **12**, 2844 (2021).
- [59] M.-Y. Li, Y. Shi, C.-C. Cheng, L.-S. Lu, Y.-C. Lin, H. Tang, M. Tsai, C. Chu, K. Wei, J.-H. He, W.-H. Chang, K. Suenaga, and L.-J. Li, Epitaxial growth of a monolayer WSe₂-MoS₂ lateral *p-n* junction with an atomically sharp interface, *Science* **349**, 524 (2015).
- [60] P. K. Sahoo, S. Memaran, Y. Xin, L. Balicas, and Humberto R. Gutiérrez, One-pot growth of two-dimensional lateral heterostructures via sequential edge-epitaxy, *Nature* **553**, 63 (2018).
- [61] Z. Zhang, P. Chen, X. Duan, K. Zang, J. Luo, and X. Duan, Robust epitaxial growth of two-dimensional heterostructures, multiheterostructures, and superlattices, *Science* **357**, 788 (2017).
- [62] R. Ramesh and D. G. Schlom, Creating emergent phenomena in oxide superlattices, *Nat. Rev. Mater.* **4**, 257 (2019).
- [63] R. C. Haislmaier, Greg Stone, N. Alem, and R. Engel-Herbert, Creating Ruddlesden-Popper phases by hybrid molecular beam epitaxy, *Appl. Phys. Lett.* **109**, 043102 (2016).
- [64] M. T. Suzuki, T. Nomot, R. Arita, Y. Yanagi, S. Hayami, and H. Kusunose, Multipole expansion for magnetic structures: A generation scheme for a symmetry-adapted orthonormal basis set in the crystallographic point group, *Phys. Rev. B* **99**, 174407 (2019).
- [65] T. Nagamiya, S. Tomiyoshi, and Y. Yamaguchi, Triangular spin configuration and weak ferromagnetism of Mn₃Sn and Mn₃Ge, *Solid State Commun.* **42**, 385 (1982).
- [66] P. J. Brown, V. Nunez, F. Tasset, J. Forsyth, and P. Radhakrishna, Determination of the magnetic structure of Mn₃Sn using generalized neutron polarization analysis, *J. Phys.: Condens. Matter* **2**, 9409 (1990).

- [67] H. Chen, Q. Niu, and A. H. MacDonald, Anomalous Hall effect arising from noncollinear antiferromagnetism, *Phys. Rev. Lett.* **112**, 017205 (2014).
- [68] J. Kübler and C. Felser, Noncollinear antiferromagnets and the anomalous Hall effect, *EPL* **108**, 67001 (2014).
- [69] S. Nakatsuji, N. Kiyohara, and T. Higo, Large anomalous Hall effect in a noncollinear antiferromagnet at room temperature, *Nature* **527**, 212 (2015).
- [70] J. Železný, Y. Zhang, C. Felser, and B. Yan, Spin-polarized current in noncollinear antiferromagnets, *Phys. Rev. Lett.* **119**, 187204 (2017).
- [71] G. Gurung, D.-F. Shao, and E. Y. Tsymbal, Transport Spin Polarization of Noncollinear Antiferromagnetic Antiperovskites, *Phys. Rev. Mater.* **5**, 124411 (2021).
- [72] Y.-P. Zhu, X. Chen, X.-R. Liu, Y. Liu, P. Liu, H. Zha, G. Qu, C. Hong, J. Li, Z. Jiang, X.-M. Ma, Y.-J. Hao, M.-Y. Zhu, W. Liu, M. Zeng, S. Jayaram, M. Lenger, J. Ding, S. Mo, K. Tanaka, M. Arita, Z. Liu, M. Ye, D. Shen, J. Wrachtrup, Y. Huang, R.-H. He, S. Qiao, Q. Liu, and C. Liu, Observation of plaid-like spin splitting in a noncoplanar antiferromagnet, arXiv:2303.04549 (2023).
- [73] G. Gurung, D.-F. Shao, and E. Y. Tsymbal, Transport spin polarization of noncollinear antiferromagnetic antiperovskites, *Phys. Rev. Mater.* **5**, 124411 (2021).
- [74] G. Gurung, D.-F. Shao, and E. Y. Tsymbal, Extraordinary tunneling magnetoresistance in antiferromagnetic tunnel junctions with antiperovskite electrodes, arXiv:2306.03026 (2023).
- [75] S. Hu, D.-F. Shao, H. Yang, C. Pan, Z. Fu, M. Tang, Y. Yang, W. Fan, S. Zhou, E. Y. Tsymbal, and X. Qiu, Efficient perpendicular magnetization switching by a magnetic spin Hall effect in a noncollinear antiferromagnet, *Nat. Commun.* **13**, 4447 (2022).
- [76] H. Tsai, T. Higo, K. Kondou, T. Nomoto, A. Sakai, A. Kobayashi, T. Nakano, K. Yakushiji, R. Arita, and S. Miwa, Electrical manipulation of a topological antiferromagnetic state, *Nature* **580**, 608 (2020).
- [77] T. Higo, K. Kondou, T. Nomoto, M. Shiga, S. Sakamoto, X. Chen, D. Nishio-Hamane, R. Arita, Y. Otani, S. Miwa, and S. Nakatsuji, Perpendicular full switching of chiral antiferromagnetic order by current, *Nature* **607**, 474–479 (2022).
- [78] T. Xu, H. Bai, Y. Dong, L. Zhao, H.-A. Zhou, J. Zhang, X.-X. Zhang, and W. Jiang, Robust spin torque switching of noncollinear antiferromagnet Mn_3Sn , *APL Mater.* **11**, 071116 (2023).
- [79] Y. Deng, X. Liu, Y. Chen, Z. Du, N. Jiang, C. Shen, E. Zhang, H. Zheng, H.-Z. Lu, and K. Wang, All-electrical switching of a topological noncollinear antiferromagnet at room temperature, *Natl. Sci. Rev.* **10**, nwac154 (2023).
- [80] P. Lukashev, R. F. Sabirianov, and K. Belashchenko, Theory of the piezomagnetic effect in Mn-based antiperovskites, *Phys. Rev. B* **78**, 184414 (2008).
- [81] D.-F. Shao, G. Gurung, T. R. Paudel, and E. Y. Tsymbal, Electrically reversible magnetization at the antiperovskite/perovskite interface, *Phys. Rev. Materials* **3**, 024405 (2019).
- [82] J. C. Slonczewski, Current-driven excitation of magnetic multilayers, *J. Magn. Magn. Matter* **159**, L1 (1996).
- [83] A. Brataas, A. D. Kent, and H. Ohno, Current-induced torques in magnetic materials, *Nat. Mater.* **11**, 372 (2012).
- [84] D. Ralph and M. Stiles, Spin transfer torques, *J. Magn. Magn. Matter.* **320**, 1190 (2008).
- [85] I. M. Miron, G. Gaudin, S. Auffret, B. Rodmacq, A. Schuhl, S. Pizzini, J. Vogel, and P. Gambardella, Current-driven spin torque induced by the Rashba effect in a ferromagnetic metal layer, *Nat. Mater.* **9**, 230 (2010).
- [86] I. M. Miron, K. Garello, G. Gaudin, P.-J. Zermatten, M. V. Costache, S. Auffret, S. Bandiera, B. Rodmacq, A. Schuhl, and P. Gambardella, Perpendicular switching of a single ferromagnetic layer induced by in-plane current injection, *Nature* **476**, 189 (2011).
- [87] L. Liu, C.-F. Pai, Y. Li, H. W. Tseng, D. C. Ralph, and R. A. Buhrman, Spin-torque switching with the giant spin Hall effect of tantalum, *Science* **336**, 555 (2012).
- [88] A. Manchon, J. Zelezný, I. M. Miron, T. Jungwirth, J. Sinova, A. Thiaville, K. Garello, and P. Gambardella, Current-induced spin-orbit torques in ferromagnetic and antiferromagnetic systems, *Rev. Mod. Phys.* **91**, 035004 (2019).
- [89] S. Zhang, P. M. Levy, and A. Fert, Mechanisms of spin-polarized current-driven magnetization switching, *Phys. Rev. Lett.* **88**, 236601 (2002).
- [90] R. Cheng, M. W. Daniels, J.-G. Zhu, and D. Xiao, Ultrafast switching of antiferromagnets via spin-transfer torque, *Phys. Rev. B* **91**, 064423 (2015).
- [91] O. V. Gomonay and V. M. Loktev, Spin transfer and current-induced switching in antiferromagnets, *Phys. Rev. B* **81**, 144427 (2010).
- [92] O. Gomonay, V. Baltz, A. Brataas, and Y. Tserkovnyak, Antiferromagnetic spin textures and dynamics, *Nat. Phys.* **14**, 213 (2018).
- [93] J. Železný, H. Gao, K. Výborný, J. Zemen, J. Mašek, A. Manchon, J. Wunderlich, J. Sinova, and T. Jungwirth, Relativistic Néel-order fields induced by electrical current in antiferromagnets, *Phys. Rev. Lett.* **113**, 157201 (2014).
- [94] P. Wadley, B. Howells, J. Železný, C. Andrews, V. Hills, R. P. Campion, V. Novák, K. Olejník, F. Maccherozzi, S. S. Dhesi, S. Y. Martin, T. Wagner, J. Wunderlich, F. Freimuth, Y. Mokrousov, J. Kuneš, J. S. Chauhan, M. J. Grzybowski, A. W. Rushforth, K. W. Edmonds, B. L. Gallagher, and T. Jungwirth, Electrical switching of an antiferromagnet, *Science* **351**, 587 (2016).
- [95] X. Z. Chen, R. Zarzuela, J. Zhang, C. Song, X. F. Zhou, G. Y. Shi, F. Li, H. A. Zhou, W. J. Jiang, F. Pan, and Y. Tserkovnyak, Antidamping-torque-induced switching in biaxial antiferromagnetic insulators, *Phys. Rev. Lett.* **120**, 207204 (2018).
- [96] S. Ghosh, A. Manchon, and J. Železný, Unconventional robust spin-transfer torque in noncollinear antiferromagnetic junctions, *Phys. Rev. Lett.* **128**, 097702 (2022).
- [97] L. Baldrati, O. Gomonay, A. Ross, M. Filianina, R. Lebrun, R. Ramos, C. Leveille, F. Fuhrmann, T. R. Forrest, F. MacCherozzi, S. Valencia, F. Kronast, E. Saitoh, J. Sinova, and M. Klau, Mechanism of Néel order switching in antiferromagnetic thin films revealed by magnetotransport and direct imaging, *Phys. Rev. Lett.* **123**, 177201 (2019).
- [98] P. Zhang, C.-T. Chou, H. Yun, B. C. McGoldrick, J. T. Hou, K. A. Mkhoyan, and L. Liu, Control of Néel vector with spin-orbit torques in an antiferromagnetic insulator with tilted easy plane, *Phys. Rev. Lett.* **129**, 017203 (2022).
- [99] H. Bai, Y. C. Zhang, L. Han, Y. J. Zhou, F. Pan, and C. Song, Antiferromagnetism: An efficient and controllable spin source, *Appl. Phys. Rev.* **9**, 041316 (2022).

- [100] Q. Liu, Y. Guo, and A. J. Freeman, Tunable Rashba Effect in Two-Dimensional LaOBiS₂ Films: Ultrathin Candidates for Spin Field Effect Transistors, *Nano Lett.* **13**, 5264(2013).
- [101] X. Zhang, Q. Liu, J.-W. Luo, A. J. Freeman, and A. Zunger, Hidden spin polarization in inversion-symmetric bulk crystals, *Nat. Phys.* **10**, 387 (2014).
- [102] X. F. Zhou, J. Zhang, F. Li, X. Z. Chen, G. Y. Shi, Y. Z. Tan, Y. D. Gu, M. S. Saleem, H. Q. Wu, F. Pan, and C. Song, Strong orientation-dependent spin-orbit torque in thin films of the antiferromagnet Mn₂Au, *Phys. Rev. Appl.* **9**, 054028 (2018).
- [103] D. -F. Shao, G. Gurung, S. -H. Zhang, and E. Y. Tsymbal, Dirac nodal line metal for topological antiferromagnetic spintronics, *Phys. Rev. Lett.* **122**, 077203 (2019).
- [104] X. Jia, K. Xia, Y. Ke, and H. Guo, Nonlinear bias dependence of spin-transfer torque from atomic first principles, *Phys. Rev. B* **84**, 014401 (2011).
- [105] H. Fujita, Field-free spin-current control of magnetization in noncollinear chiral antiferromagnets, *Phys. Stat. Sol. RRL* **11**, 1600360 (2017).
- [106] G. Gurung, D.-F. Shao, and E. Y. Tsymbal, Spin-torque switching of noncollinear antiferromagnetic antiperovskites, *Phys. Rev. B* **101**, 140405(R) (2020).
- [107] Y. Yamane, O. Gomonay, and J. Sinova, Dynamics of noncollinear antiferromagnetic textures driven by spin current injection, *Phys. Rev. B* **100**, 054415 (2019).
- [108] D. Go, M. Sallermann, F. R. Lux, S. Blügel, O. Gomonay, and Y. Mokrousov, Noncollinear spin current for switching of chiral magnetic textures, *Phys. Rev. Lett.* **129**, 097204 (2022).
- [109] R. González-Hernández, P. Ritzinger, K. Výborný, J. Železný, and A. Manchon, Non-relativistic torque and Edelstein effect in noncollinear magnets, arXiv:2310.06499 (2023).
- [110] Z. Xu, X. Zhang, Y. Qiao, G. Liang, S. Shi, and Z. Zhu, Deterministic spin-orbit torque switching of Mn₃Sn with the interplay between spin polarization and Kagome plane, arXiv:2308.08091 (2023).
- [111] S. Y. Bodnar, L. Šmejkal, I. Turek, T. Jungwirth, O. Gomonay, J. Sinova, A. A. Sapozhnik, H.-J. Elmers, M. Kläui, and M. Jourdan, Writing and reading antiferromagnetic Mn₂Au by Néel spin-orbit torques and large anisotropic magnetoresistance, *Nat. Commun.* **9**, 348 (2018).
- [112] C. C. Chiang, S. Y. Huang, D. Qu, P. H. Wu, and C. L. Chien, Absence of evidence of electrical switching of the antiferromagnetic Néel vector, *Phys. Rev. Lett.* **123**, 227203 (2019).
- [113] J. Fischer, O. Gomonay, R. Schlitz, K. Ganzhorn, N. Vlietstra, M. Althammer, H. Huebl, M. Opel, R. Gross, S. T. B. Goennenwein, and S. Geprägs, Spin Hall magnetoresistance in antiferromagnet/heavy-metal heterostructures, *Phys. Rev. B* **97**, 014417 (2018).
- [114] S. P. Bommanaboyena, D. Backes, L. S. I. Veiga, S. S. Dhesi, Y. R. Niu, B. Sarpi, T. Denneulin, A. Kovács, T. Mashoff, O. Gomonay, J. Sinova, K. Everschor-Sitte, D. Schönte, R. M. Reeve, M. Kläui, H.-J. Elmers, and M. Jourdan, Readout of an antiferromagnetic spintronics system by strong exchange coupling of Mn₂Au and permalloy, *Nat. Commun.* **12**, 6539 (2021).
- [115] A. Du, D. Zhu, K. Cao, Z. Zhang, Z. Guo, K. Shi, D. Xiong, R. Xiao, W. Cai, J. Yin, S. Lu, C. Zhang, Y. Zhang, S. Luo, A. Fert, and W. Zhao, Electrical manipulation and detection of antiferromagnetism in magnetic tunnel junctions, *Nat. Electron.* **6**, 425 (2023).
- [116] I. Dzyaloshinsky, A thermodynamic theory of “weak” ferromagnetism of antiferromagnetics, *J. Phys. Chem. Solids* **4**, 4 (1958).
- [117] T. Moriya, Anisotropic superexchange interaction and weak ferromagnetism, *Phys. Rev.* **120**, 91 (1960).
- [118] S.-S. Zhang, Z.-A. Wang, B. Li, S.-H. Zhang, R.-C. Xiao, L.-X. Liu, X. Luo, W. J. Lu, M. Tian, Y. P. Sun, E. Y. Tsymbal, H. Du, and D.-F. Shao, X-type antiferromagnets, arXiv: 2310.13271 (2023).
- [119] X. Chen, X. Zhou, R. Cheng, C. Song, J. Zhang, Y. Wu, Y. Ba, H. Li, Yi. Sun, Y. You, Y. Zhao and F. Pan, Electric field control of Néel spin-orbit torque in an antiferromagnet, *Nat. Mater.* **18**, 931 (2019).
- [120] H. Yan, Z. Feng, S. Shang, X. Wang, Z. Hu, J. Wang, Z. Zhu, H. Wang, Z. Chen, H. Hua, W. Lu, J. Wang, P. Qin, H. Guo, X. Zhou, Z. Leng, Z. Liu, C. Jiang, M. Coey, and Z. Liu, A piezoelectric, strain-controlled antiferromagnetic memory insensitive to magnetic fields, *Nat. Nanotechnol.* **14**, 131 (2019).
- [121] J. T. Heron, D. G. Schlom, and R. Ramesh, Electric field control of magnetism using BiFeO₃-based heterostructures, *Appl. Phys. Rev.* **1**, 021303 (2014).
- [122] D. Yi, J. Liu, S. Okamoto, S. Jagannatha, Y.-C. Chen, P. Yu, Y.-H. Chu, E. Arenholz, R. Ramesh, Tuning the competition between ferromagnetism and antiferromagnetism in a half-doped manganite through magnetoelectric coupling, *Phys. Rev. Lett.* **111**, 127601 (2013).
- [123] D. Yi, P. Yu, Y. Chen, H. H. Lee, Q. He, Y. H. Chu and R. Ramesh, Tailoring magnetoelectric coupling in BiFeO₃/La_{0.7} Sr_{0.3} MnO₃ by engineering interfacial polar discontinuity, *Adv. Mater.* **31**, 1806335 (2019).
- [124] X. He, Y. Wang, N. Wu, A. N. Caruso, E. Vescovo, K. D. Belashchenko, P. A. Dowben, and C. Binek, Robust isothermal electric control of exchange bias at room temperature, *Nat. Mater.* **9**, 579 (2010).
- [125] V. Lopez-Dominguez, H. Almasi, and P. Khalili Amiri, Picosecond electric-field-induced switching of antiferromagnets, *Phys. Rev. Applied* **11**, 024019 (2019).
- [126] J. Yuan, Y. Song, X. Xing, and J. Chen, Magnetic structure and uniaxial negative thermal expansion in antiferromagnetic CrSb, *Dalton Trans.* **49**, 17605 (2020).
- [127] M. Ijjaali, B. Malaman, C. Gleitzer, J. K. Warner, J. A. Hriljac, and A.K. Cheetham, Stability, structure refinement, and magnetic properties of β -Fe₂(PO₄)O, *J. Solid State Chem.* **86**, 195 (1990).
- [128] Y. Guo, H. Liu, O. Janson, I. C. Fulga, J. van den Brink, and J. I. Facio, Spin-split collinear antiferromagnets: A large-scale ab-initio study, *Mater. Today Phys.* **32**, 100991 (2023).
- [129] Z.-F. Gao, S. Qu, B. Zeng, Y. Liu, J.-R. Wen, H. Sun, P. -J. Guo, Z.-Y. Lu, AI-accelerated discovery of altermagnetic materials, arXiv:2311.04418 (2023).
- [130] P. P. Freitas, R. Ferreira, and S. Cardoso, Spintronic sensors, *Proc. IEEE* **104**, 1894 (2016).
- [131] D.-F. Shao, S.-H. Zhang, R.-C. Xiao, Z.-A. Wang, W. J. Lu, Y. P. Sun, and E. Y. Tsymbal, Spin-neutral tunneling anomalous Hall effect, *Phys. Rev. B* **106**, L180404 (2022).
- [132] A. Matos-Abiague and J. Fabian, Tunneling anomalous and spin Hall effects, *Phys. Rev. Lett.* **115**, 056602 (2015).
- [133] B. Scharf, A. Matos-Abiague, J. E. Han, E. M. Hankiewicz, and I. Žutić, Tunneling planar Hall effect in topological insulators:

- Spin valves and amplifiers, *Phys. Rev. Lett.* **117**, 166806 (2016).
- [134] J. Moser, A. Matos-Abiad, D. Schuh, W. Wegscheider, J. Fabian, and D. Weiss, Tunneling anisotropic magnetoresistance and spin-orbit coupling in Fe/GaAs/Au tunnel junctions, *Phys. Rev. Lett.* **99**, 056601 (2007).
- [135] W. Chen, M. Gu, J. Li, P. Wang, and Q. Liu, Role of hidden spin polarization in nonreciprocal transport of antiferromagnets, *Phys. Rev. Lett.* **129**, 276601 (2022).